

Article

Supramolecular Detection of a Nerve Agent Simulant by Fluorescent Zn–Salen Oligomer Receptors

Roberta Puglisi ^{1,*}, Placido G. Mineo ^{1,2}, Andrea Pappalardo ^{1,3}, Antonino Gulino ^{1,3}  and Giuseppe Trusso Sfrassetto ^{1,3,*} 

¹ Department of Chemical Sciences, University of Catania, Viale A. Doria 6, 95100 Catania, Italy; gmineo@unict.it (P.G.M.); andrea.pappalardo@unict.it (A.P.); agulino@unict.it (A.G.)

² CNR-IPCB Istituto per i Polimeri, Compositi e Biomateriali, Via P. Gaifami 18, I-95126 Catania, Italy

³ Department of Chemical Sciences, University of Catania Research Unit (I.N.S.T.M.) UdR of Catania, Viale A. Doria 6, 95125 Catania, Italy

* Correspondence: r.puglisi@unict.it (R.P.); giuseppe.trusso@unict.it (G.T.S.); Tel.: +39-09-5738-5201 (G.T.S.)

Academic Editor: Antonella Dalla Cort

Received: 3 May 2019; Accepted: 7 June 2019; Published: 8 June 2019



Abstract: We report on new Zn–Salen oligomer receptors able to recognize a nerve agent simulant, namely dimethyl methylphosphonate (DMMP), by a supramolecular approach. In particular, three Zn–Salen oligomers (Zn–Oligo–A, –B, and –C), differing by the length distribution, were obtained and characterized by NMR, Gel Permeation Chromatography (GPC), UV-Vis, and fluorescence spectroscopy. Furthermore, we investigated their recognition properties towards DMMP by using fluorescence measurements. We found that the recognition ability depends on the length of the oligomeric chain, and the Zn–Oligo–C shows a binding constant value higher than those already reported in literature for the DMMP detection.

Keywords: chemical warfare agents; supramolecular detection; oligo–Salen

1. Introduction

The nerve agents (NAs) of G and V series (Figure 1) are the most toxic known organophosphorus (OP) derivatives, synthesized for the first time as pesticides and then used as chemical weapons during world conflicts or terroristic attacks. They are strong acetylcholinesterase inhibitors and cause cholinergic crisis in the human body, after breath exposure [1,2].

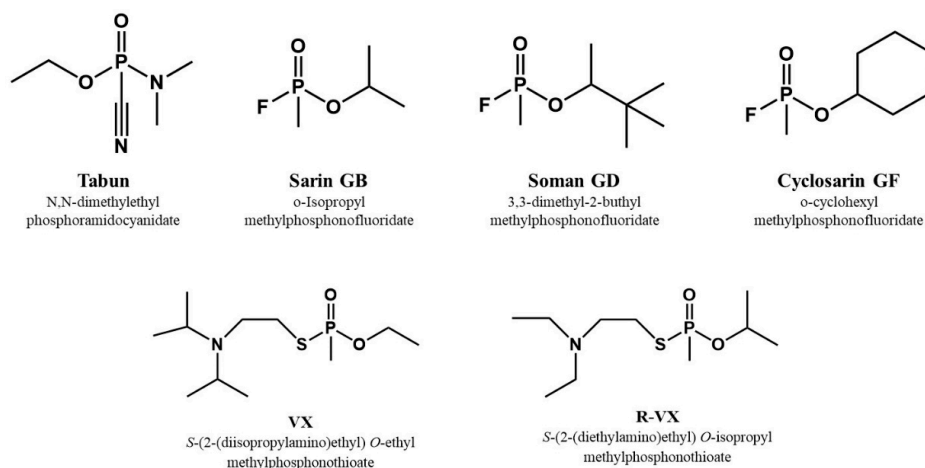


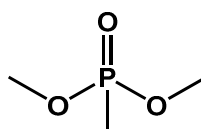
Figure 1. Nerve agents of G (top) and V (bottom) series.

G-series NAs are highly volatile (for example, Tabun, Sarin, and Soman show a volatility in the 576–22,000 mg/m³ range at 25 °C), while the V-series shows lower volatility (3–30 mg/m³ at 25 °C). For these reasons, NA can be released in air or in water. These compounds start to be toxic in the 25–400 mg × min/m³ range. For these reasons, a good sensor should be able to detect NA both in solution and in gas phase, with a detection limit of few ppm.

Although use, synthesis, and storage of chemical warfare agents (CWAs) are forbidden for security reasons, OP compounds, such as Sarin, Soman, and the more recent Novichock [3] are still used as weapons to injure or kill people, as demonstrated by some recent international events [4,5].

With the aim to increase human health and safety, many efforts have been made to develop new and more efficient detection systems, able to reveal the presence of OP compounds in low concentrations and to give a measurable and observable response of NA presence [6].

Due to their high toxicity, the use of nerve agents is not even allowed for research activity. For this reason, studies on new molecular receptors are carried out using simulants—less toxic organophosphorus compounds. In this context, recent studies demonstrated that dimethyl methylphosphonate (DMMP, Figure 2) is one of the best simulants for “G” series nerve agents [7].



DMMP
Dimethyl
methylphosphonate

Figure 2. DMMP structure.

Instrumental recognition of nerve gases (such as mass spectrometry or gas chromatography) is highly sensitive [8,9]. However, the complexity of the systems involved is a limit for a “real field” application. In this context, molecular probes represent a more convenient detection strategy [10]. Today, molecular sensing of chemical warfare agents can be performed by two main different methods: (i) A covalent approach, in which the receptor covalently binds the analyte, thus giving a measurable response (such as a change of the fluorescence emission) after the interaction [11,12]. Due to the nature of the interactions involved, covalent receptors are not reusable after a first exposure to nerve agents, and false positive responses can be obtained; (ii) the more recent and less studied supramolecular approach to detect NA by non-covalent reversible interactions, thus leading to a supramolecular reversible host–guest complex and reusable sensors [13].

To date, only a few examples of supramolecular hosts for CWA simulants have been reported in the literature [14–24]. They exploit several non-covalent interactions for the recognition of the guest, such as inclusion within the hydrophobic macrocyclic cavity [14–17] or hydrogen bond-dependent gel formation [18–25].

Metal–Salen complexes are well known in literature for their use as catalysts [26–30] and supramolecular hosts [31–38], where the Lewis acid metal center is exploited for the recognition of Lewis base species. Furthermore, recently we also demonstrated the high efficiency of metal–Salen complexes as receptors for NA simulants [25,39]. In particular, we reported on uranyl–Salen complexes able to efficiently recognize DMMP with high affinity constants due to a Lewis acid–base interaction between the metal center and the phosphate group [25]. In order to obtain a fluorescence response, we explored the use of Zn–Salen complexes for the DMMP detection, and achieved excellent results in terms of affinity and selectivity [39].

Encouraged by these results, in this work we investigated both the multivalence effect [40], derived from the use of a large number of available recognition sites linked to each other in Zn–Salen chains, and the additivity effect of the individual binding contribution in the detection of DMMP. To the best

of our knowledge, this is the first example of oligomer-based Salen able to detect CWA simulants in solution.

To this aim, we reported here the synthesis, characterization, and DMMP recognition abilities of three different Zn–Salen oligomers (Zn–Oligo–A, –B, and –C, Figure 3), differing by the length of the oligomeric chain.

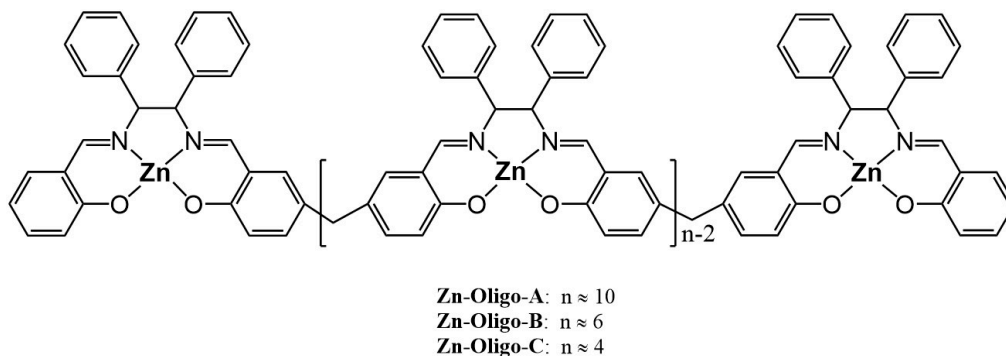
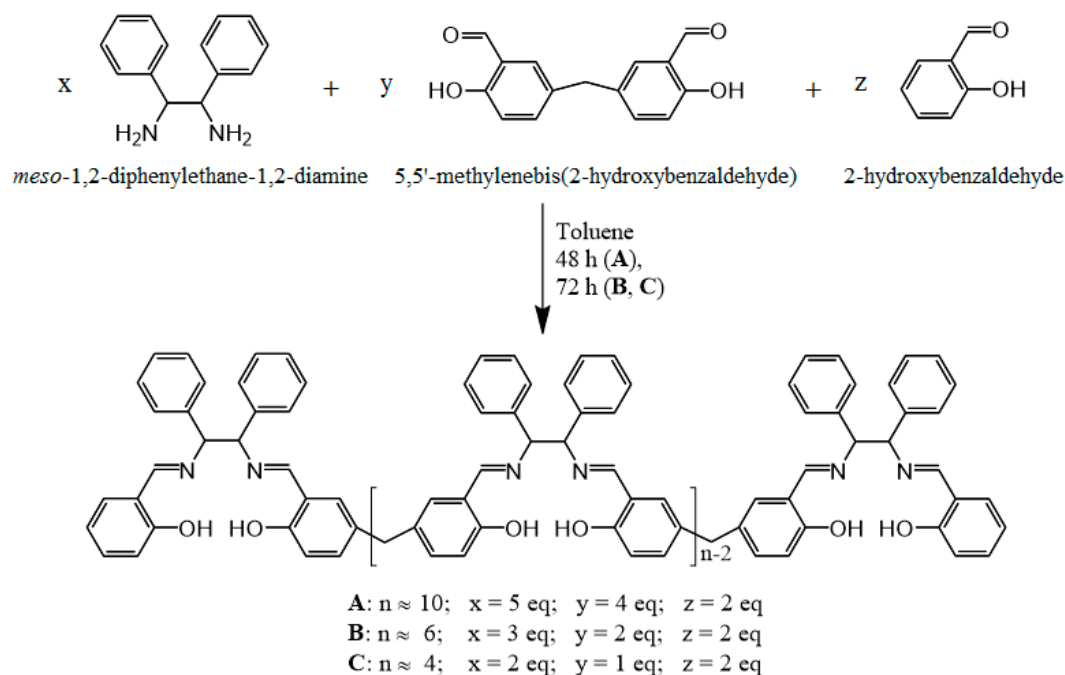


Figure 3. Schematic representation of the Zn–Salen oligomer hosts.

2. Results and Discussion

Oligo–Salen ligands A, B, and C were easily synthesized in a one pot reaction, by mixing the proper ratios of (1,2–diphenyl)–ethylenediamine (x), 5,5′–methylenebis(2–hydroxybenzaldehyde) (y) [41], and 2–hydroxybenzaldehyde in toluene (z) (Scheme 1). The role of 2–hydroxybenzaldehyde in toluene is crucial to tune the length of the oligomeric chain.



Scheme 1. Schematic reaction pathways of the Oligo–Salen ligands.

The reactions were monitored by TLC (Thin Layer Chromatography), following the disappearance of the starting reagent. The total conversions were reached after 48 h for A, 72 h for B and C. The oligo–Salen ligands A, B, and C were isolated by evaporation of the solvent and treatment with *n*-hexane. The isolated compounds showed similar ^1H NMR spectra (Figure 4).

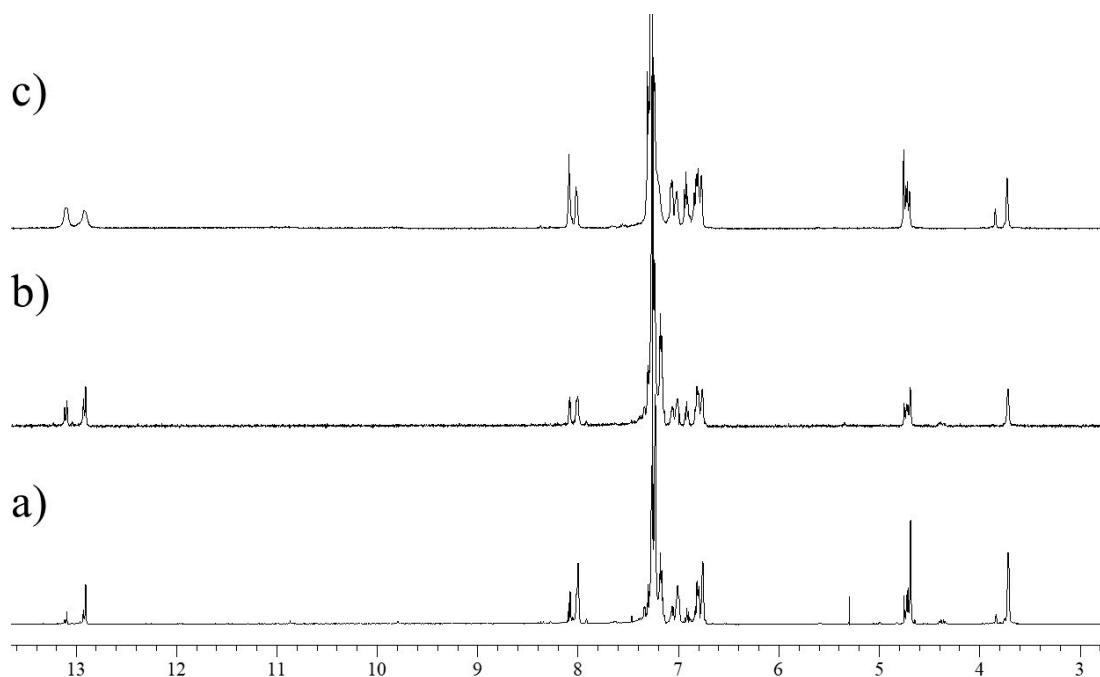


Figure 4. ^1H NMR spectra in CDCl_3 of: (a) Oligo-Salen-A; (b) Oligo-Salen-B; (c) Oligo-Salen-C.

In particular, the following characteristic pattern of signals suggested the formation of the typical Salen backbone (Figure 5): (i) The disappearance of the aldehydic signal at ca. 10 ppm, (ii) the presence of signals at 8 ppm relative to the imine proton (β in Figure 5), and (iii) the downfield shift of hydroxyl protons signals, from 10.9 [41] to 13 ppm (α in Figure 5). In addition, the presence of methine (χ in Figure 5) and methylene protons (γ in Figure 5) at 4.8 and 3.7 ppm, respectively, confirmed the presence of the oligomeric chains.

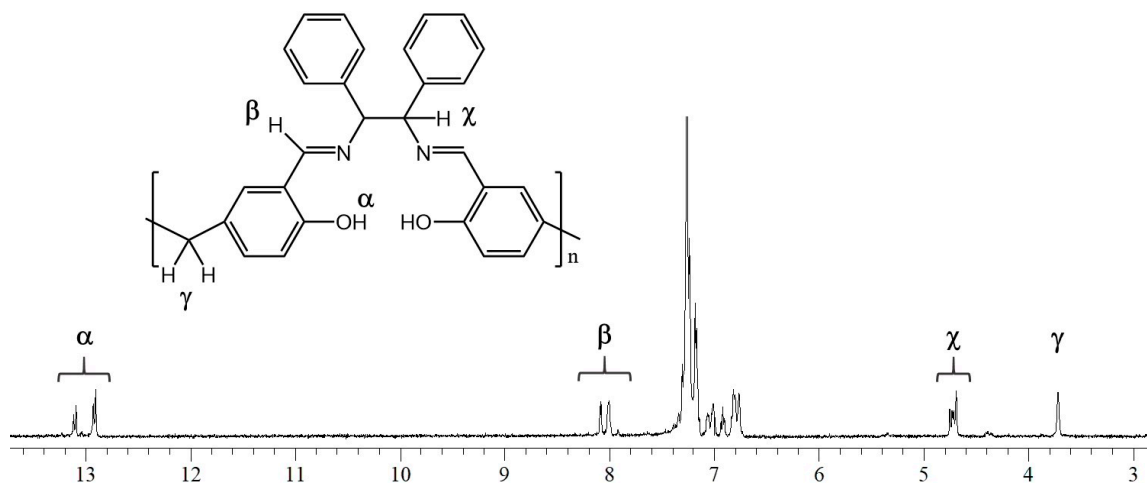


Figure 5. Representative ^1H NMR spectrum of the Oligo-Salen-B (reported in the inset) in CDCl_3 .

Diffusion order spectroscopy is a useful NMR technique that can provide information about dimensions of analyzed species, measuring the diffusion coefficient [42,43]. DOSY measurements conducted in CDCl_3 showed a diffusion coefficient of $3.41 \times 10^{-10} \text{ m}^2\text{s}^{-1}$ for the Oligo-Salen-A ($1 \times 10^{-3} \text{ M}$) corresponding to an estimated molecular mass of 4650 Da, thus suggesting the prevailing presence of an oligomer containing ten units. Similarly, both Oligo-Salen-B and Oligo-Salen-C were analyzed by DOSY experiments in the same experimental conditions, and showed diffusion coefficients of $4.23 \times 10^{-10} \text{ m}^2\text{s}^{-1}$ and $5.29 \times 10^{-10} \text{ m}^2\text{s}^{-1}$, respectively. These data suggest the prevalent formation

(in the oligomer mixtures) of a hexameric species for the Oligo–Salen–B and a tetrameric species for the Oligo–Salen–C (see Table 1).

Table 1. DOSY results.

Oligomer ^a	D ($\times 10^{-10} \text{ m}^2\text{s}^{-1}$)	Calcd. Mn ^b	Degree of Polymerization ^c
Oligo–Salen–A	3.41	4650	~10
Oligo–Salen–B	4.23	2760	~6
Oligo–Salen–C	5.29	1640	~4

^a Concentration of sample = 1×10^{-3} M in CDCl_3 ; ^b estimated by using the method described in Ref. [41]; ^c Degree of polymerization = $M_n/M_{R,U}$.

In addition, ^1H NMR spectra showed two patterns of signals relative to imine and OH groups: The downfield signals were related to the terminal aldehydic moiety of the oligomeric chain, while the upfield signals were relative to the inner core of the chain. The relative integration of these signals supported the identification performed by DOSY and Gel Permeation Chromatography GPC measurements.

To confirm the oligomeric nature of the obtained products and the decreasing of the averaging molecular weight by varying the reagents' molar ratio, several GPC experiments were performed.

In particular, the GPC traces of the Oligo–Salen–A, –B and –C oligomeric mixtures (Figure 6) showed partially resolved peaks in the elution volume range 14.5–21.5 mL, certainly due to the presence of oligomeric species. It can be noticed that upon decreasing the amine/aldehyde molar ratio, the mass distribution curve moves toward higher elution volumes with, as expected, a quantitative enrichment of the oligomers at lower molar mass.

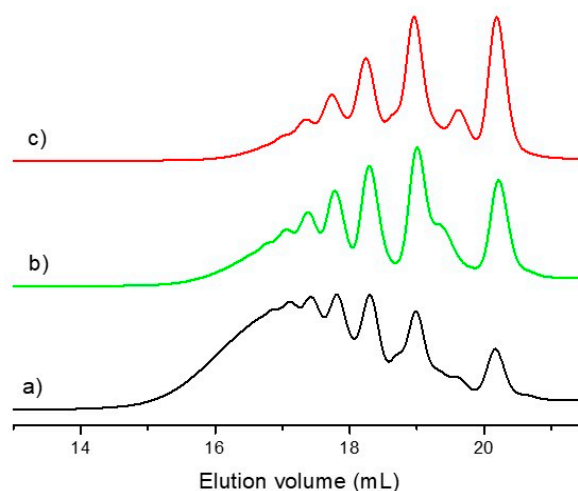
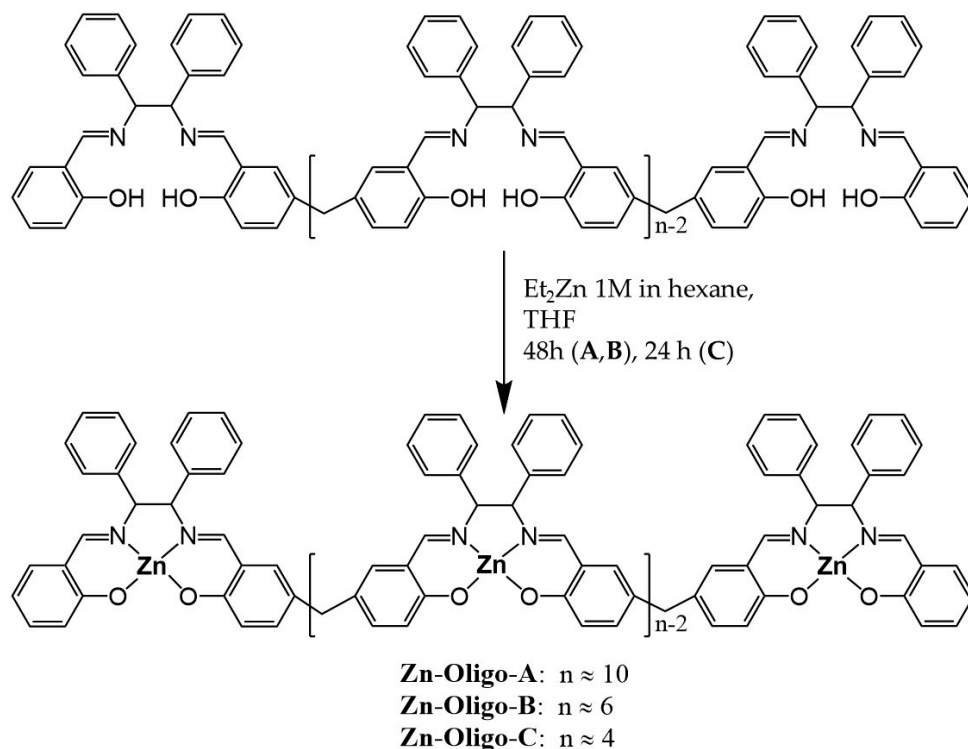


Figure 6. GPC traces of the Oligo–Salen–A, –B and –C compounds: (a) Oligo–Salen–A; (b) Oligo–Salen–B; (c) Oligo–Salen–C.

The oligomeric structures of the products were also confirmed by means of MALDI-TOF MS (see for example the spectrum of the Oligo–Salen–C reported in Figure S18 in the Supplementary Materials). This spectrum mainly consists of a series of peaks at m/z $851 + n432$ ($n = 0-7$), detected as protonated species ($[\text{MH}]^+$), that can be assigned to the molecular species reported in the inset of Figure 5.

Metalation reactions of the three different Oligo–Salen compounds were performed in THF, by adding Zinc–Diethyl 1 M in hexane (Scheme 2) and collecting the final Zinc–Salen–oligomer complexes by filtration. ^1H NMR spectra recorded in $\text{DMSO}-d_6$ of Zn–Oligo–A, –B, and –C were similar. In particular, they showed a common upfield shift of the imine proton signals and the absence of hydroxyl group signals, thus supporting the formation of metal complexes.



Scheme 2. Synthesis of Zn-Salen oligomer hosts.

UV-Vis absorbance spectra of oligomers showed the azomethine transition bands at ca. 325 nm (Figure 7a). Additionally, the corresponding Zn complexes showed similar profiles, with one main band consistent with the $n-\pi^*$ transitions (Figure 7b). In particular, the spectrum of Zn-Oligo-A recorded in DMSO showed a broad band at 365.2 nm ($\epsilon = 10,000 \text{ cm}^{-1} \text{ M}^{-1}$). Similarly, in the absorption spectrum of Zn-Oligo-B in DMSO, this band appeared at 372.0 nm ($\epsilon = 10,050 \text{ cm}^{-1} \text{ M}^{-1}$), while in the UV-Vis spectrum of Zn-Oligo-C it lay at 370.0 nm ($\epsilon = 14,600 \text{ cm}^{-1} \text{ M}^{-1}$).

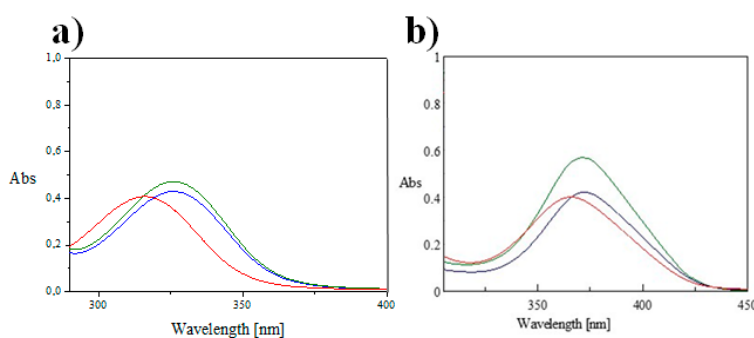


Figure 7. (a) UV-Vis spectra of Oligo-Salen-A (red), Oligo-Salen-B (blue), and Oligo-Salen-C (green) in DMSO ($4 \times 10^{-5} \text{ M}$); (b) Zn-Oligo-A (red), Zn-Oligo-B (blue), and Zn-Oligo-C (green) in DMSO ($4 \times 10^{-5} \text{ M}$).

Emission properties of Zn-oligomers were studied in DMSO. Using an excitation wavelength of 365 nm, similar fluorescence spectra were observed for all the three Zn-oligomers, with an intense emission band centered at ca. 480 nm (see Figure 8). The emission quantum yields calculated for the oligomers ($\varphi = 0.31, 0.47, \text{ and } 0.64$ for Zn-Oligo-A, -B, and -C, respectively) showed a clear dependence on the length of the chains. The large Stokes shift (more than 100 nm) observed for these receptors paves the way for their sensing application.

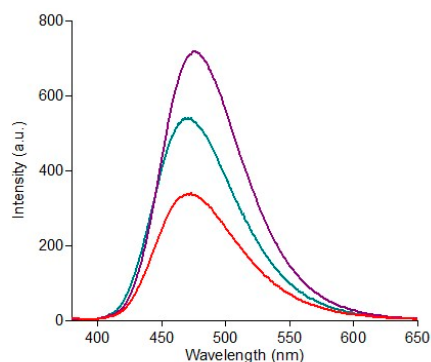


Figure 8. Emission spectra of Zn-Oligo-A (red), Zn-Oligo-B (green), and Zn-Oligo-C (purple) in DMSO (1×10^{-5} M, $\lambda_{\text{ex}} = 365$ nm).

Recognition studies of the three receptors towards DMMP were conducted by following the progressive quenching of the emission intensity, probably due to a PET (Photoinduced Electron Transfer) mechanism [44], upon the addition of DMMP to a solution of each receptor (Figure 9a–c). As reported in Figure 9d, Zn-Oligo-C showed the highest emission quenching after the addition of DMMP. The limit of detection was $1 \mu\text{M}$ with all the receptors. The sensibility of Zn-Oligo hosts for DMMP is shown in Figure 9d, which highlighted the possibility to detect ppm (part per million) of DMMP. In particular, 1 ppm of DMMP produced an intensity emission variation of 25%–30%, if normalized with respect to the total observed variation, in Zn-Oligo-A and –C. This variation reached more than 70% with 10 ppm in the case of Zn-Oligo-C. Figure 9e shows the supramolecular complex proposed between Zn-oligomers and DMMP, supported by our previous studies in which 2D-NMR measurements suggested supramolecular geometry [39].

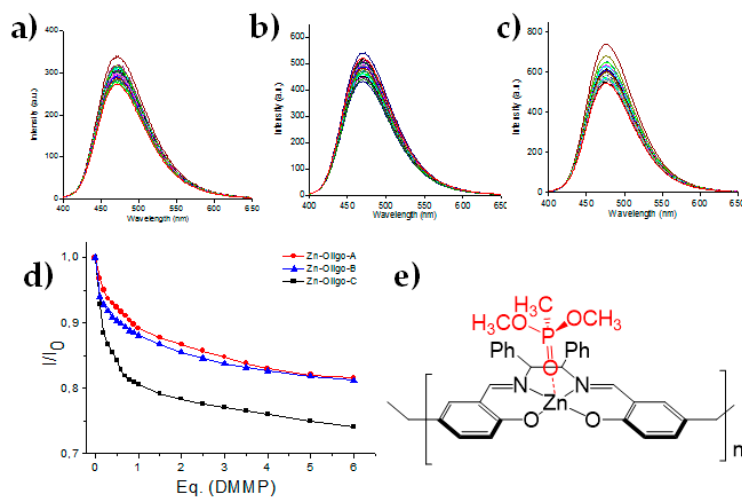


Figure 9. Fluorescence emission spectra of (a) Zn-Oligo-A, (b) Zn-Oligo-B, and (c) Zn-Oligo-C upon progressive addition of 0–6 eq. of DMMP ([receptors] = 1×10^{-5} M in DMSO, λ_{ex} 365 nm); (d) normalized fluorescence emission variation relative to Zn-Oligo-A (red), –B (blue), and –C (black) solutions (1×10^{-5} M in DMSO, λ_{ex} 365 nm), upon addition of DMMP (0–6 eq.); (e) supramolecular host–guest complex proposed.

The data treatment using the HypSpec software provided the binding constant values for each receptor. Non-linear curve fit plots were performed by using a 1:1 stoichiometry, supported by our previous studies on CWA recognition by Metal–Salen complexes [31–37]. Interestingly, moving from longer to shorter oligomer distribution, an increase of the affinity was observed (see Table 2). In particular, we found that Zn-Oligo-C showed the highest affinity constant value towards DMMP and this value was larger than those already reported in the literature, even if compared with the

monomeric form previously studied [39], due to the multivalence effect. However, the higher binding constant value of Zn–Oligo–C with respect to the longer receptors could be ascribed to energetic contributions. In particular, due to the presence in the oligomeric chain of the methylene groups, the shorter host could be more preorganized for the host–guest complex formation with respect to the longer receptors, which contains more methylene bridges.

Table 2. Binding constant values of oligomeric and monomeric receptors, towards DMMP in DMSO solution.

Guest: DMMP	Zn–Oligo–A	Zn–Oligo–B	Zn–Oligo–C	Zn–5- <i>t</i> but (Monomer)
LogK ^a	4.86	4.98	5.69	4.33 [39]

^a calculated using HypSpec 1.1.33.

Moreover, selectivity and competition tests were performed for the Zn–Oligo–C. In particular, atmospheric air (containing 24,000 ppm of water, 400 ppm CO₂, 5 ppm NO, and 10 ppm CO) was bubbled for 10 min into a 1×10^{-5} M DMSO solution of Zn–Oligo–C. The emission spectra of the host were acquired before and after air bubbling, thus finding that the emission profile did not change after air exposure (see the Supplementary Materials). This experiment demonstrated that the emission properties of Zn–Oligo–C was not affected by the analytes/contaminants contained in the air. Then, this air-saturated solution was exposed to DMMP and we observed a decrease of the emission, thus confirming the ability of Zn–Oligo–C to also recognize DMMP in competitive conditions (see the Supplementary Materials).

In order to evaluate the use of Zn–Oligo–C as a real sensor, a preliminary test strip was carried out. Common filter paper was adsorbed with the Zn–Oligo–C solution (50 μ L, 1 mM in DMSO). After the exposure to DMMP vapors (40 ppm, in a closed vial at room temperature), a clear decrease of color intensity was observed (Figure 10). This preliminary result paves the way for the employment of this new receptor as a sensor prototype.

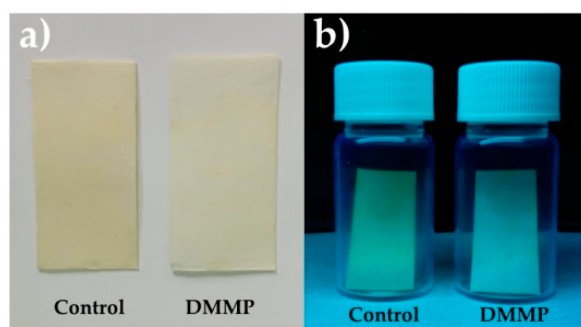


Figure 10. Test strip on filter paper (2.5×3 cm) adsorbed with the Zn–Oligo–C solution (1×10^{-3} M in DMSO), before (Control) and after (DMMP) the exposure to DMMP vapors (a 20 mL vial containing 1 μ L of DMMP 0.1 M in CH₂Cl₂): (a) Under daylight; (b) under UV lamp irradiation (365 nm).

3. Materials and Methods

General experimental methods. The NMR experiments were carried out at 27 °C on a Varian UNITY Inova 500 MHz spectrometer (¹H at 499.88 MHz, Varian-Agilent, Santa Clara, CA, USA) equipped with pulse field gradient module (Z axis) and a tunable 5 mm Varian inverse detection probe (ID-PFG). A JASCO V-560 UV-Vis spectrophotometer (Mettler Toledo, Novate Milanese, Italy) equipped with a 1 cm path-length cell was used for the UV-Vis measurements. Luminescence measurements were carried out using a Cary Eclipse Fluorescence spectrophotometer (Agilent, Santa Clara, CA, USA) with resolution of 0.5 nm, at room temperature. The emission was recorded at 90° with respect to the exciting line beam using 10:5 slit-widths for all measurements. The fluorescence quantum yields were calculated by using *N*-butyl-4-butylamino-1,8-naphthalimide as standard. All chemicals were reagent

grade and used without further purification. ^{13}C NMR characterizations of oligomers were precluded due to the scarce solubility of the compounds.

Gel permeation chromatography. A PL-GPC 110 (Polymer Laboratories) thermostat system, equipped with three PL-gel 5 mm columns (two Mixed-D and one Mixed-E) attached in series, was used. The analyses were performed at 35 ± 0.1 °C using THF as eluent at a flow rate of 1 mL/min. A differential refractometer (Polymer Laboratories, Wyatt Technology, Dernbach, Germany) was used as detector.

Procedure for epsilon calculation. UV-Vis spectra of four solutions of the hosts at different concentration, from 1×10^{-5} M to 4×10^{-5} M, were measured at 25 °C. Data treatment allowed for the calculation of epsilon for each absorption band.

Procedure for fluorescence titrations. Two stock solutions of host and guest (1.0×10^{-3} M) in dry solvent were prepared. From these, progressive amounts of guest solution were added to the host (from 0 to 6 eq.), and emission spectra were recorded at 25 °C. Fluorescence titration with Zn-Oligo-A, -B, and -C were carried out using $\lambda_{\text{ex}} = 365$ nm in dry DMSO and recorded at $\lambda_{\text{em}} = 480$ nm at 25 °C. With this data treatment, the apparent binding affinities of receptors with DMMP were estimated using the HypSpec (version 1.1.33, Protonic Software, Florence, Italy) [45,46], a software designed to extract equilibrium constants from potentiometric and/or spectrophotometric titration data. HypSpec starts with an assumed complex formation scheme and uses a least-squares approach to derive the spectra of the complexes and the stability constants. χ^2 test (chi-square) was applied, where the residuals follow a normal distribution (for a distribution approximately normal, the χ^2 test value is around 12 or less). In all of the cases, values of $\chi^2 \leq 10$ were found, as obtained by 3 independent measurements sets.

DOSY experiments. Diffusion Ordered Spectroscopy (DOSY) NMR was used to determine the presence of monomeric or higher species in solution. The DOSY technique provides information about the size of the molecular aggregate in solution. Furthermore, the diffusion coefficient value could be associated to the molecular weight by the mathematic treatment recently described [42,43]. DOSY experiments on Oligo-Salen-A in DMSO- d_6 (10 mM) showed a diffusion coefficient of $3.41 \times 10^{-10} \text{ m}^2 \text{ s}^{-1}$, corresponding to a calculated molecular weight of ca. 4650 (prevalence of decameric form, the experimental molecular weight of dimer is 4330). While in DMSO- d_6 , a solution of Oligo-Salen-B (10 mM) showed a diffusion coefficient of $4.23 \times 10^{-10} \text{ m}^2 \text{ s}^{-1}$, (calculated molecular weight of 2760, prevalence of hexameric form, the experimental molecular weight is 2598). Oligo-Salen-C showed a diffusion coefficient of $5.29 \times 10^{-10} \text{ m}^2 \text{ s}^{-1}$ (calculated molecular weight of 1640, prevalence of tetrameric form, the experimental molecular weight is 1732), relative to a solution of ligand in DMSO- d_6 (10 mM).

Synthesis of Oligo-Salen-A: 5,5'-methylenebis-2-hydroxybenzaldehyde (0.150 g, 0.58 mmol) [39], 2-hydroxy-benzaldehyde (31 μL , 0.29 mmol), and *meso*-1,2-diphenylethylenediamine (0.160 g, 0.73 mmol) were stirred in anhydrous toluene (22 mL) at room temperature for 48 h. Then the solvent was removed under reduced pressure, thus leading to the Oligo-Salen-A (0.380 g) as pale yellow crystals, then washed with hexane: ^1H NMR (500MHz, CDCl_3) δ 13.1–12.8 (bs, 2H, OH), 8.1–7.9 (m, 2H, CH=N), 7.4–6.6 (m, 18H, ArH), 4.8–4.6 (bs, 2H, Ar-CH-N), 3.7 (bs, 2H, Ar-CH₂-Ar) ppm. Anal. Calcd. for $\text{C}_{290}\text{H}_{260}\text{N}_{20}\text{O}_{20}$: C, 80.16; H, 6.03; N, 6.45. Found C, 80.12; H, 6.01; N, 6.41.

Synthesis of Oligo-Salen-B: 5,5'-methylenebis-2-hydroxybenzaldehyde (0.150 g, 0.58 mmol), 2-hydroxy-benzaldehyde (62 μL , 0.58 mmol), and *meso*-1,2-diphenylethylenediamine (0.192 g, 0.87 mmol) were stirred in anhydrous toluene (22 mL) at room temperature for 72 h. Then the solvent was removed under reduced pressure, thus leading to the Oligo-Salen-B (0.230 g) as pale yellow crystals, then washed with hexane: ^1H NMR (500MHz, CDCl_3) δ 13.1–12.8 (bs, 2H, OH), 8.1–7.9 (m, 2H, CH=N), 7.4–6.7 (m, 18H, ArH), 4.8–4.6 (bs, 2H, Ar-CH-N), 3.7 (bs, 2H, Ar-CH₂-Ar) ppm. Anal. Calcd. for $\text{C}_{174}\text{H}_{156}\text{N}_{12}\text{O}_{12}$: Found C, 80.14; H, 6.00; N, 6.39.

Synthesis of Oligo-Salen-C: 5,5'-methylenebis-2-hydroxybenzaldehyde (39 mg, 0.15 mmol), 2-hydroxy-benzaldehyde (32 μL , 0.30 mmol), and *meso*-1,2-diphenylethylenediamine (66 mg, 0.30 mmol) were stirred in anhydrous toluene (22 mL) at room temperature for 72 h. Then the solvent

was removed under reduced pressure, thus leading to the Oligo–Salen–C (40 mg) as yellow crystals, then washed with hexane: ^1H NMR (500MHz, CDCl_3) δ 13.1–12.8 (bs, 2H, OH), 8.1–7.9 (m, 2H, CH=N), 7.4–6.7 (m, 18H, ArH), 4.8–4.6 (bs, 2H, Ar-CH-N), 3.7 (bs, 2H, Ar-CH₂-Ar) ppm. Anal. Calcd. for $\text{C}_{116}\text{H}_{104}\text{N}_8\text{O}_8$: Found C, 80.11; H, 6.02; N, 6.44.

Synthesis of Zn–Oligo–A: To a solution of the Oligo–Salen–A ligand 0.315 g (0.73 mmol) in dry tetrahydrofuran (15 mL), 900 μL (0.90 mmol) of Et_2Zn 1 M in hexane was added. The reaction mixture was stirred for 48 h at room temperature, thus affording Zn–Oligo–A (0.350 g) as a brown-yellow precipitate, which was collected by filtration. ^1H NMR (500MHz, CDCl_3) δ 8.2–8.0 (m, 2H, H-C=N), 7.2–6.3 (m, 17H, Ar-H), 5.1–5.0 (m, 2H, Ar-CH-N), 3.5 (bs, 2H, Ar-CH₂-Ar) ppm. Anal. Calcd. for $\text{C}_{290}\text{H}_{240}\text{N}_{20}\text{O}_{20}\text{Zn}_{10}$: C, 69.96; H, 4.86; N, 5.63. Found C, 69.92; H, 4.81; N, 5.60.

Synthesis of Zn–Oligo–B: To a solution of Oligo–Salen–B ligand 0.200 g (0.46 mmol) in dry tetrahydrofuran (19 mL), 680 μL (0.60 mmol) of Et_2Zn 1 M in hexane was added. The reaction mixture was stirred for 48 h at room temperature, thus affording Zn–Oligo–B (0.190 g) as a brown-yellow precipitate, which was collected by filtration. ^1H NMR (500MHz, CDCl_3) δ 8.2–8.0 (m, 2H, H-C=N), 7.3–6.3 (m, 17H, Ar-H), 5.1–4.9 (m, 2H, Ar-CH-N), 3.5 (bs, 2H, Ar-CH₂-Ar) ppm. Anal. Calcd. for $\text{C}_{174}\text{H}_{144}\text{N}_{12}\text{O}_{12}\text{Zn}_6$: Found C, 69.93; H, 4.85; N, 5.59.

Synthesis of Zn–Oligo–C: Oligo–Salen–C ligand (38 mg, 0.080 mmol) was dissolved in dry tetrahydrofuran (6 mL). To this solution, 100 μL (0.10 mmol) of Et_2Zn 1 M in hexane was added. The reaction mixture was stirred for 24 h at room temperature, thus affording Zn–Oligo–C (23 mg) as a yellow precipitate, which was collected by filtration. ^1H NMR (500MHz, CDCl_3) δ 8.2–8.0 (m, 2H, H-C=N), 7.3–6.3 (m, 17H, Ar-H), 5.1–5.0 (m, 2H, Ar-CH-N), 3.5 (bs, 2H, Ar-CH₂-Ar) ppm. Anal. Calcd. for $\text{C}_{116}\text{H}_{96}\text{N}_8\text{O}_8\text{Zn}_4$: Found C, 69.91; H, 4.80; N, 5.55.

4. Conclusions

In this manuscript we describe the synthesis and characterization of three new Zn–oligomer–based Salen complexes. The easy synthetic protocols based on the mixing of reagents with a proper stoichiometric ratio allowed for the obtainment of oligomers with four, six, and ten Salen units. These oligomers were tested as receptors for DMMP and we found excellent results with the shorter oligomer. In fact, the shorter oligomer showed the highest binding constant value with respect to the other sensors used for the non-covalent detection of DMMP. These results suggest the possibility to employ the oligomer hosts in the CWA detection, in order to obtain final solid devices with higher affinity for the analytes.

Supplementary Materials: The following are available online at <http://www.mdpi.com/1420-3049/24/11/2160/s1>: NMR, UV-Vis, emission spectra, fluorescence titration.

Author Contributions: P.G.M. performed GPC analysis; A.P. and A.G. analyzed the data; R.P. and G.T.S. designed the experiments and wrote the paper.

Funding: This research was funded by University of Catania—Department of Chemical Science (Piano per la Ricerca Linea Intervento 2).

Acknowledgments: Dedicated to Prof. Gaetano A. Tomaselli and Prof. Francesco P. Ballistreri in occasion of their retirement.

Conflicts of Interest: The authors declare no conflicts of interest.

References

1. Romano, J.A., Jr.; Lukey, B.J.; Salem, H. *Chemical Warfare Agents Chemistry, Pharmacology, Toxicology, and Therapeutics*, 2nd ed.; Taylor & Francis Group: Oxfordshire, UK, 2007.
2. Mercey, G.; Verdelet, T.; Renou, J.; Kliachyna, M.; Baati, R.; Nachon, F.; Jean, L.; Renard, P.-Y. Reactivators of Acetylcholinesterase Inhibited by Organophosphorus Nerve Agents. *Acc. Chem. Res.* **2012**, *45*, 756–766. [[CrossRef](#)] [[PubMed](#)]
3. Vale, J.A.; Marrs, T.C.; Maynard, R.L. Novichok: A murderous nerve agent attack in the UK. *Clin. Toxicol.* **2018**, *56*, 1093–1097. [[CrossRef](#)] [[PubMed](#)]

4. Stone, R. U.K. attack puts nerve agent in the spotlight. *Science* **2018**, *359*, 1314–1315. [[CrossRef](#)] [[PubMed](#)]
5. Stone, R. How to defeat a nerve agent. *Science* **2018**, *359*, 23. [[CrossRef](#)] [[PubMed](#)]
6. Kim, K.; Tsay, O.G.; Atwood, D.A.; Churchill, D.G. Destruction and Detection of Chemical Warfare Agents. *Chem. Rev.* **2011**, *111*, 5345–5403. [[CrossRef](#)]
7. Lavoie, J.; Srinivasan, S.; Nagarajan, R. Using cheminformatics to find simulants for chemical warfare agents. *J. Hazard. Mater.* **2011**, *194*, 85–91. [[CrossRef](#)]
8. Ohru, Y.; Nagoya, T.; Kurimata, N.; Sodeyama, M.; Seto, Y. Identification of V-type nerve agents in vapor samples using a field-portable capillary gas chromatography/membrane-interfaced electron ionization quadrupole mass spectrometry instrument with Tri-Bed concentrator and fluoridating conversion tube. *J. Mass Spectrom.* **2017**, *52*, 472–479. [[CrossRef](#)]
9. Tak, V.; Purohit, A.; Pardasani, D.; Goud, D.R.; Jain, R.; Dubey, D.K. Simultaneous detection and identification of precursors, degradation and co-products of chemical warfare agents in drinking water by ultra-high performance liquid chromatography-quadrupole time-of-flight mass spectrometry. *J. Chromatogr. A* **2014**, *1370*, 80–92. [[CrossRef](#)]
10. Zhou, X.; Lee, S.; Xu, Z.; Yoon, J. Recent Progress on the Development of Chemosensors for Gases. *Chem. Rev.* **2015**, *115*, 7944–8000. [[CrossRef](#)]
11. Sarkar, H.S.; Ghosh, A.; Das, S.; Maiti, P.K.; Maitra, S.; Mandal, S.; Sahoo, P. Visualisation of DCP, a nerve agent mimic, in Catfish brain by a simple chemosensor. *Sci. Rep.* **2018**, *8*, 1–7. [[CrossRef](#)]
12. Lloyd, E.P.; Pilato, R.S.; Van Houten, K.A. Polymer-Bound 4-Pyridyl-5-hydroxyethyl-thiazole Fluorescent Chemosensors for the Detection of Organophosphate Nerve Agent Simulants. *ACS Omega* **2018**, *3*, 16028–16034. [[CrossRef](#)] [[PubMed](#)]
13. Sambrook, M.R.; Notman, S. Supramolecular chemistry and chemical warfare agents: From fundamentals of recognition to catalysis and sensing. *Chem. Soc. Rev.* **2013**, *42*, 9251–9267. [[CrossRef](#)] [[PubMed](#)]
14. Tudisco, C.; Betti, P.; Motta, A.; Pinalli, R.; Bombaci, L.; Dalcanale, E.; Condorelli, G.G. Cavitand-Functionalized Porous Silicon as an Active Surface for Organophosphorus Vapor Detection. *Langmuir* **2012**, *28*, 1782–1789. [[CrossRef](#)] [[PubMed](#)]
15. Chen, S.; Ruan, Y.; Brown, J.D.; Gallucci, J.; Maslak, V.; Hadad, C.M.; Badjic, J.D. Assembly of Amphiphilic Baskets into Stimuli-Responsive Vesicles. Developing a Strategy for the Detection of Organophosphorus Chemical Nerve Agents. *J. Am. Chem. Soc.* **2013**, *135*, 14964–14967. [[CrossRef](#)] [[PubMed](#)]
16. Chen, S.; Ruan, Y.; Brown, J.D.; Hadad, C.M.; Badjic, J.D. Recognition Characteristics of an Adaptive Vesicular Assembly of Amphiphilic Baskets for Selective Detection and Mitigation of Toxic Nerve Agents. *J. Am. Chem. Soc.* **2014**, *136*, 17337–17342. [[CrossRef](#)] [[PubMed](#)]
17. Ruan, Y.; Chen, S.; Brown, J.D.; Hadad, C.M.; Badjic, J.D. Ubiquitous Assembly of Amphiphilic Baskets into Unilamellar Vesicles and Their Recognition Characteristics. *Org. Lett.* **2015**, *17*, 852–855. [[CrossRef](#)] [[PubMed](#)]
18. Grate, J.W.; Kaganove, S.N.; Patrash, S.J.; Craig, R.; Bliss, M. Hybrid Organic/Inorganic Copolymers with Strongly Hydrogen-Bond Acidic Properties for Acoustic Wave and Optical Sensors. *Chem. Mater.* **1997**, *9*, 1201–1207. [[CrossRef](#)]
19. Kim, H.J.; Lee, J.H.; Lee, H.; Lee, J.H.; Lee, J.H.; Jung, J.H.; Kim, J.S. A Mesoporous, Silica-Immobilized-Nanoparticle Colorimetric Chemosensor for the Detection of Nerve Agents. *Adv. Funct. Mater.* **2011**, *21*, 4035–4040. [[CrossRef](#)]
20. Hiscock, J.R.; Piana, F.; Sambrook, M.R.; Wells, N.J.; Clark, A.J.; Vincent, J.C.; Busschaert, N.; Brown, R.C.D.; Gale, P.A. Detection of nerve agent via perturbation of supramolecular gel formation. *Chem. Commun.* **2013**, *49*, 9119–9121. [[CrossRef](#)]
21. Ruan, Y.; Dalkilic, E.; Peterson, P.W.; Pandit, A.; Dastan, A.; Brown, J.D.; Polen, S.M.; Hadad, C.M.; Badjic, J.D. Trapping of organophosphorus chemical nerve agents in water with amino acid functionalized baskets. *Chem. Eur. J.* **2014**, *20*, 4251–4256. [[CrossRef](#)]
22. Barba-Bon, A.; Costero, A.M.; Parra, M.; Gil, S.; Martinez-Manez, R.; Sancenon, F.; Gale, P.A.; Hiscock, J.R. Neutral 1,3-Diindolylureas for Nerve Agent Remediation. *Chem. Eur. J.* **2013**, *19*, 1586–1590. [[CrossRef](#)] [[PubMed](#)]
23. Sambrook, M.R.; Hiscock, J.R.; Cook, A.; Green, A.C.; Holden, I.; Vincent, J.C.; Gale, P.A. Hydrogen bond-mediated recognition of the chemical warfare agent soman (GD). *Chem. Commun.* **2012**, *48*, 5605–5607. [[CrossRef](#)] [[PubMed](#)]

24. Puglisi, R.; Pappalardo, A.; Gulino, A.; Trusso Sfrazzetto, G. Multitopic Supramolecular Detection of Chemical Warfare Agents by Fluorescent Sensors. *ACS Omega* **2019**, *4*, 7550–7555. [[CrossRef](#)]
25. Trusso Sfrazzetto, G.; Millesi, S.; Pappalardo, A.; Tomaselli, G.A.; Ballistreri, F.P.; Toscano, R.M.; Fragalà, I.; Gulino, A. Nerve Gas Simulant Sensing by an Uranyl-Salen Monolayer Covalently Anchored on Quartz Substrates. *Chem. Eur. J.* **2017**, *23*, 1576–1583. [[CrossRef](#)] [[PubMed](#)]
26. Ballistreri, F.P.; Toscano, R.M.; Amato, M.E.; Pappalardo, A.; Gangemi, C.M.A.; Spidalieri, S.; Puglisi, R.; Trusso Sfrazzetto, G. A new Mn-Salen micellar nanoreactor for enantioselective epoxidation of alkenes in water. *Catalysts* **2018**, *8*, 129. [[CrossRef](#)]
27. Ballistreri, F.P.; Gangemi, C.M.A.; Pappalardo, A.; Tomaselli, G.A.; Toscano, R.M.; Trusso Sfrazzetto, G. (Salen)Mn(III) catalyzed asymmetric epoxidation reactions by hydrogen peroxide in water: A green protocol. *Int. J. Mol. Sci.* **2016**, *17*, 1112. [[CrossRef](#)]
28. Trusso Sfrazzetto, G.; Millesi, S.; Pappalardo, A.; Toscano, R.M.; Ballistreri, F.P.; Tomaselli, G.A.; Gulino, A. Olefin epoxidation by a (salen)Mn(III) catalyst covalently grafted on glass beads. *Catal. Sci. Technol.* **2015**, *5*, 673–679. [[CrossRef](#)]
29. La Paglia Fragola, V.; Lupo, F.; Pappalardo, A.; Trusso Sfrazzetto, G.; Toscano, R.M.; Ballistreri, F.P.; Tomaselli, G.A.; Gulino, A. A surface-confined O:MnV(salen) oxene catalyst and high turnover values in asymmetric epoxidation of unfunctionalized olefins. *J. Mater. Chem.* **2012**, *22*, 20561–20565. [[CrossRef](#)]
30. Zammataro, A.; Gangemi, C.M.A.; Pappalardo, A.; Toscano, R.M.; Puglisi, R.; Nicotra, G.; Fragalà, M.E.; Tuccitto, N.; Trusso Sfrazzetto, G. Covalently functionalized carbon nanoparticles with a chiral Mn-Salen: A new nanocatalyst for enantioselective epoxidation of alkenes. *Chem. Commun.* **2019**, *55*, 5255–5258. [[CrossRef](#)]
31. Puglisi, R.; Ballistreri, F.P.; Gangemi, C.M.A.; Toscano, R.M.; Tomaselli, G.A.; Pappalardo, A.; Trusso Sfrazzetto, G. Chiral Zn-salen complexes: A new class of fluorescent receptors for enantiodiscrimination of chiral amines. *New J. Chem.* **2017**, *41*, 911–915. [[CrossRef](#)]
32. Patti, A.; Pedotti, S.; Ballistreri, F.P.; Trusso Sfrazzetto, G. Synthesis and Characterization of Some Chiral Metal-Salen Complexes Bearing a Ferrocenophane Substituent. *Molecules* **2009**, *14*, 4312–4325. [[CrossRef](#)] [[PubMed](#)]
33. Ballistreri, F.P.; Pappalardo, A.; Tomaselli, G.A.; Toscano, R.M.; Trusso Sfrazzetto, G. A New Heteroditopic Chiral Uranyl-Salen Receptor for Molecular Recognition of Amino Acid Ammonium Salts. *Eur. J. Org. Chem.* **2010**, 3806–3810. [[CrossRef](#)]
34. Amato, M.E.; Ballistreri, F.P.; D'Agata, S.; Pappalardo, A.; Tomaselli, G.A.; Toscano, R.M.; Trusso Sfrazzetto, G. Enantioselective Molecular Recognition of Chiral Organic Ammonium Ions and Amino Acids Using Cavitand-Salen-Based Receptors. *Eur. J. Org. Chem.* **2011**, 5674–5680. [[CrossRef](#)]
35. Pappalardo, A.; Amato, M.E.; Ballistreri, F.P.; Tomaselli, G.A.; Toscano, R.M.; Trusso Sfrazzetto, G. Pair of Diastereomeric Uranyl Salen Cavitands Displaying Opposite Enantiodiscrimination of α -Amino Acid Ammonium Salts. *J. Org. Chem.* **2012**, *77*, 7684–7687. [[CrossRef](#)] [[PubMed](#)]
36. D'Urso, A.; Tudisco, C.; Ballistreri, F.P.; Condorelli, G.G.; Randazzo, R.; Tomaselli, G.A.; Toscano, R.M.; Trusso Sfrazzetto, G.; Pappalardo, A. Enantioselective extraction mediated by a chiral cavitand–salen covalently assembled on a porous silicon surface. *Chem. Commun.* **2014**, *50*, 4993–4996. [[CrossRef](#)] [[PubMed](#)]
37. Mihan, F.Y.; Bartocci, S.; Bruschini, M.; De Bernardin, P.; Forte, G.; Giannicchi, I.; Dalla Cort, A. Ion-Pair Recognition by Metal-Salophen and Metal-Salen Complexes. *Austr. J. Chem.* **2012**, *65*, 1638–1646. [[CrossRef](#)]
38. Forte, G.; D'Urso, A.; Ballistreri, F.P.; Toscano, R.M.; Tomaselli, G.A.; Trusso Sfrazzetto, G.; Pappalardo, A. Enantiomeric Recognition of α -Amino Acid Derivatives by Chiral Uranyl-Salen Receptors. *Tetrahedron Lett.* **2015**, *56*, 2922–2926. [[CrossRef](#)]
39. Puglisi, R.; Pappalardo, A.; Gulino, A.; Trusso Sfrazzetto, G. Supramolecular recognition of a CWA simulant by metal–salen complexes: The first multi-topic approach. *Chem. Commun.* **2018**, *54*, 11156–11159. [[CrossRef](#)]
40. Huskens, J.; Prins, L.J.; Haag, R.; Ravoo, B.J. *Multivalency: Concepts, Research & Applications*; Wiley and Sons: Hoboken, NJ, USA, 2018; ISBN 978-1-119-14346-8.
41. Tuccitto, N.; Amato, T.; Gangemi, C.M.A.; Trusso Sfrazzetto, G.; Puglisi, R.; Pappalardo, A.; Ballistreri, F.P.; Messina, G.M.L.; Li-Destri, G.; Marletta, G. Driving Coordination Polymer Monolayer Formation by Competitive Reactions at the Air/Water Interface. *Langmuir* **2018**, *34*, 11706–11713. [[CrossRef](#)]

42. Evans, R.; Deng, Z.; Rogerson, A.K.; McLachlan, A.S.; Richards, J.J.; Nilsson, M.; Morris, G.A. Quantitative Interpretation of Diffusion-Ordered NMR Spectra: Can We Rationalize Small Molecule Diffusion Coefficients? *Angew. Chem. Int. Ed.* **2013**, *52*, 3199–3202. [[CrossRef](#)]
43. Giuffrida, M.L.; Rizzarelli, E.; Tomaselli, G.A.; Satriano, C.; Trusso Sfrazzetto, G. A novel fully water-soluble Cu(I) probe for fluorescence live cell imaging. *Chem. Commun.* **2014**, *50*, 9835–9838. [[CrossRef](#)] [[PubMed](#)]
44. Trusso Sfrazzetto, G.; Satriano, C.; Tomaselli, G.A.; Rizzarelli, E. Synthetic fluorescent probes to map metallostatics and intracellular fate of zinc and copper. *Coord. Chem. Rev.* **2016**, *311*, 125–167. [[CrossRef](#)]
45. Jennings, A.R.; Son, D.Y. Efficient synthesis and anion recognition of a colorimetric preorganized tripodal thiourea compound. *Tetrahedron Lett.* **2012**, *53*, 2181–2184. [[CrossRef](#)]
46. Pappalardo, A.; Ballistreri, F.P.; Li Destri, G.; Mineo, P.G.; Tomaselli, G.A.; Toscano, R.M.; Trusso Sfrazzetto, G. Supramolecular Polymer Networks Based on Calix[5]arene Tethered Poly(p-phenyleneethynylene). *Macromolecules* **2012**, *45*, 7549–7556. [[CrossRef](#)]

Sample Availability: Samples of the Zn–Oligomers are available from the authors.



© 2019 by the authors. Licensee MDPI, Basel, Switzerland. This article is an open access article distributed under the terms and conditions of the Creative Commons Attribution (CC BY) license (<http://creativecommons.org/licenses/by/4.0/>).